

Faraday Rotation Measure Synthesis for Magnetic Fields of Galaxies

P. Frick¹, D. Sokoloff², R. Stepanov¹, and R. Beck³

¹ *Institute of Continuous Media Mechanics, Korolyov str. 1, 614013 Perm, Russia*

² *Department of Physics, Moscow University, 119899, Moscow, Russia*

³ *Max-Planck-Institut für Radioastronomie, Auf dem Hügel 69, 53121 Bonn, Germany*

Accepted 2010 Received 2010; in original form 2010

ABSTRACT

RM Synthesis was recently developed as a new tool for the interpretation of polarized emission data in order to separate the contributions of different sources lying on the same line of sight. Until now the method was mainly applied to discrete sources in Faraday space (Faraday screens). Here we consider how to apply RM Synthesis to reconstruct the Faraday dispersion function, aiming at the further extraction of information concerning the magnetic fields of extended sources, e.g. galaxies. The main attention is given to two related novelties in the method, i.e. the symmetry argument in Faraday space and the wavelet technique.

We give a relation between our method and the previous applications of RM Synthesis to point-like sources. We demonstrate that the traditional RM Synthesis for a point-like source indirectly implies a symmetry argument and, in this sense, can be considered as a particular case of the method presented here. Investigating the applications of RM Synthesis to polarization details associated with small-scale magnetic fields, we isolate an option which was not covered by the ideas of the Burn theory, i.e. using quantities averaged over small-scale fluctuations of magnetic field and electron density. We describe the contribution of small-scale fields in terms of Faraday dispersion and beam depolarization. We consider the complex polarization for RM Synthesis without any averaging over small-scale fluctuations of magnetic field and electron density and demonstrate that it allows us to isolate the contribution from small-scale field.

A general conclusion concerning the applicability of RM Synthesis to the interpretation of the radio polarization data for extended sources, like galaxies, is that quite severe requirements (in particular to the wavelength range covered by observations) are needed to recognize at least the principal structure of the Faraday dispersion function. If the wavelength range of observations is not adequate we describe which features of this function can be reconstructed.

Key words: Methods: polarization – methods: data analysis – galaxies: magnetic fields – RM Synthesis – wavelets

1 INTRODUCTION

RM Synthesis is a new tool for the interpretation of polarized emission data in order to get information on the emitting media (Brentjens & de Bruyn 2005). Until now the method was mainly applied to discrete sources in Faraday space (“Faraday screens”) (Heald 2009). The aim of this paper is to discuss applications to sources which are extended in Faraday space.

RM Synthesis is based on the fact that the complex polarized intensity P can be calculated as a Fourier transform

$$P(\lambda^2) = \int_{-\infty}^{\infty} F(\phi) e^{2i\phi\lambda^2} d\phi \quad (1)$$

of the Faraday dispersion function F in Faraday space with the co-ordinate ϕ which is the Faraday depth (Burn 1966). Performing the inverse Fourier transform of P one obtains F which is the polarized

intensity emerging from a region with Faraday depth ϕ . Faraday depth is defined as

$$\phi(x) = 0.81 \int_0^x B_{\parallel}(x') n_e(x') dx', \quad (2)$$

where B_{\parallel} is the line-of-sight magnetic field component measured in μG , n_e is the thermal electron density measured in cm^{-3} and the integral is taken from the observer to the current point x along the line of sight over the region which contains both magnetic fields and thermal electrons, where x' is measured in parsecs. A convention is that ϕ is positive when \mathbf{B} is pointing towards the Earth.

In the context of RM Synthesis, one has to distinguish between Faraday depth and Faraday rotation measure RM which is defined as

$$RM(\lambda) = \frac{d\Psi}{d(\lambda^2)}, \quad (3)$$

where Ψ is the polarization angle ($P = |P|e^{2i\Psi}$).

The inversion of formula (1) shows that the Faraday dispersion function F is the Fourier transform of the complex polarized intensity:

$$F(\phi) = \frac{1}{\pi} \hat{P}(k), \quad (4)$$

where $k = 2\phi$, and the Fourier transform is defined as

$$\hat{f}(k) = \int_{-\infty}^{\infty} f(y) e^{-iky} dy. \quad (5)$$

The practical limitation of the use of Eq. (4) comes from the fact that P can be measured only for $\lambda^2 > 0$ and in only in a finite spectral band (Brown et al. 2009).

The lower bound λ_{\min} restricts the possibility to recognize objects which are extended in Faraday space, the upper bound λ_{\max} suppresses the visibility of small-scale structures of the object in Faraday space, and the lack of negative λ^2 impedes the correct reconstruction of the intrinsic polarization angle. Poor sampling inside the observations window prevent the reconstruction of objects at large Faraday depths. All these problems and limitations can also be illustrated using the wavelet representation, which provides a kind of local Fourier transform, isolating a given structure on both sides of the Fourier transform.

The topic of this paper is a further development of the wavelet approach as suggested by Frick et al. (2010) which presented at least a partial resolution of these difficulties. The paper is organized as follows. In Sects. 2,3 we describe the wavelet-based RM Synthesis and the effect of extending P to negative λ^2 , and in Sect 4 we compare RM-CLEAN (Heald 2009) to a wavelet-based RM deconvolution. We subsequently describe a few simplistic, but reasonable models of magnetic fields and electron densities in galaxy discs. Large-scale features are described in Sect. 5, small-scale features in Sect. 7. The effect of frequency coverage on reconstruction fidelity is discussed in Sect. 6. We subject these models to traditional RM Synthesis and to our wavelet approach in Sect. 8 and summarize our results in Sect. 9.

2 WAVELET-BASED RM SYNTHESIS

The wavelet transform of the Faraday dispersion function $F(\phi)$ can be written in the form

$$w_F(a, b) = \frac{1}{|a|} \int_{-\infty}^{\infty} F(\phi) \psi^* \left(\frac{\phi - b}{a} \right) d\phi, \quad (6)$$

where $\psi(\phi)$ is the analyzing wavelet, a defines the scale and b defines the position of the wavelet center. Then the coefficient w_F gives the contribution of the corresponding structure of scale b at position a to the function F .

The contribution of the complex polarized intensity to the wavelet decomposition of the Faraday dispersion function can be divided in two parts $w_F(a, b) = w_-(a, b) + w_+(a, b)$, which are defined by $P(\lambda^2)$ in negative and positive domain λ^2 , correspondingly. From Eqs. (4) and (6) one gets

$$w_+(a, b) = \frac{1}{\pi} \int_0^{\infty} P(\lambda^2) e^{-2ib\lambda^2} \hat{\psi}^* (-2a\lambda^2) d\lambda^2. \quad (7)$$

The coefficients $w_+(a, b)$ are calculated from the known $P(\lambda^2)$ for $\lambda^2 > 0$. Frick et al. (2010) suggested to recognize the dominating structures in the map $|w_+(a, b)|$. The coordinate b of the corresponding maximum gives the position ϕ_0 of the structure in Faraday

depth. Then, the coefficients $w_-(a, b)$ can be reconstructed, following the symmetry arguments (see Eq. (15) below)

$$w_-(a, b) = w_+(a, 2\phi_0(a, b) - b), \quad (8)$$

where the function $\phi_0(a, b)$ takes on a value of b which corresponds to the maximum of the dominant structure near point (a, b) . Distribution of $|w_+(a, b)|$ is usually complex and applying of Eq. (8) can be nontrivial procedure. We suggest it in Secs. 6 and 8 how to proceed in some particular cases.

The function F can be restored using the inverse transform

$$F(\phi) = \frac{1}{C_\psi} \int_{-\infty}^{\infty} \int_{-\infty}^{\infty} \psi \left(\frac{\phi - b}{a} \right) w_F(a, b) \frac{da db}{a^2}. \quad (9)$$

We use below the so-called Mexican hat $\psi(\phi) = (1 - \phi^2) \exp(-\phi^2/2)$ as the analyzing wavelet. The wavelet is real, however, the function P is complex, so the wavelet coefficients w_F are complex as well. For the chosen wavelet $w_F(-a, b) = w_F(a, b)$ and $C_\psi = 1$.

3 ROTATION MEASURE SPREAD FUNCTION

The Faraday dispersion function $\tilde{F}(\phi)$ obtained by RM Synthesis can be related to the true Faraday dispersion function $F(\phi)$ by $R(\phi)$, the ‘‘RM Spread Function’’ (RMSF) is

$$\tilde{F}(\phi) = F(\phi) * R(\phi), \quad (10)$$

where $*$ denotes the convolution. The RMSF is defined as

$$R(\phi) = K \int_{-\infty}^{\infty} W(\lambda^2) e^{-2i\phi\lambda^2} d\lambda^2, \quad (11)$$

where $W(\lambda^2)$ is the shape of the observable window in λ^2 space (the window function, which can include weights due to different sensitivities (gains) in the observation channels, see Heald (2009)) and K is a normalization constant.

For a single spectral window ($W \equiv 1$ for $\lambda_{\min} < \lambda < \lambda_{\max}$ and $W \equiv 0$ elsewhere) the RMSF has the simple form

$$R(\phi) = K e^{-2i\phi\lambda_0^2} \frac{\sin(\phi\Delta\lambda^2)}{\phi}, \quad (12)$$

where $\lambda_0^2 = (\lambda_{\min}^2 + \lambda_{\max}^2)/2$ and $\Delta\lambda^2 = (\lambda_{\max}^2 - \lambda_{\min}^2)/2$. $R(\phi)$ is shown in Fig. 1a for $\lambda_0^2 = 3.91 \text{ m}^2$ and $\Delta\lambda^2 = 2.35 \text{ m}^2$ (corresponding to the LOFAR wavelength range in the highband).¹ The RMSF usually is a complex-valued function which means that the obtained Faraday function differs from the true one not only in amplitude, but also in phase. (Due the lack of data in the domain of negative λ^2 RM Synthesis rotates the phase of the function under reconstruction.) To avoid this, Brentjens & de Bruyn (2005) proposed to multiply Eq. (12) by the factor $e^{2i\phi\lambda_0^2}$ which means that

$$R_{BB}(\phi) = K \int_{-\infty}^{\infty} W(\lambda^2) e^{-2i\phi(\lambda^2 - \lambda_0^2)} d\lambda^2 = K \frac{\sin(\phi\Delta\lambda^2)}{\phi} \quad (13)$$

and

$$\tilde{F}(\phi) = e^{-2i\phi\lambda_0^2} F(\phi) * R_{BB}(\phi). \quad (14)$$

¹ For the sake of definiteness, we consider here and below as a typical example the observational range in the LOFAR high band ($1.25 < \lambda < 2.5 \text{ m}$, see Röttgering 2003) and use another observational range if required to illustrate particular properties of RM Synthesis.

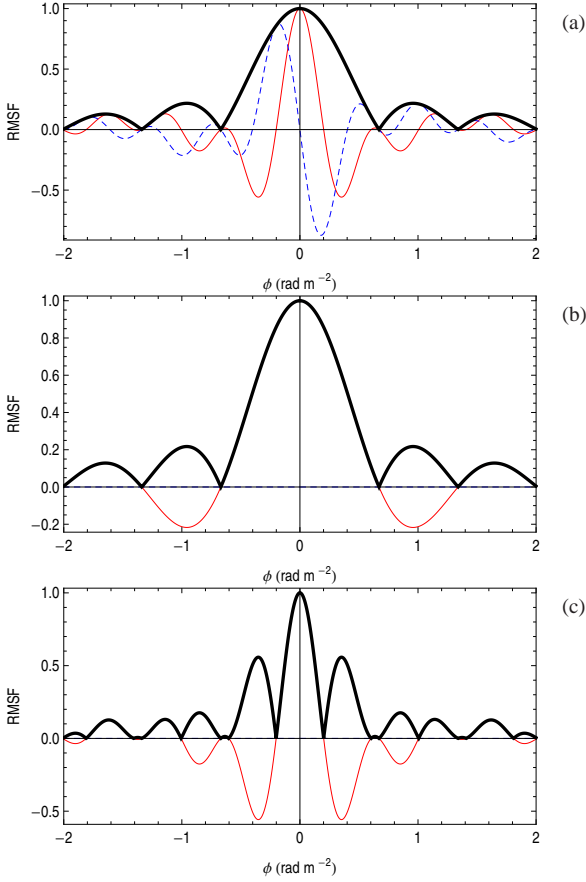


Figure 1. RM spread functions for a single observation window with $1.25 < \lambda < 2.5$ m. Panel (a): standard R ; panel (b) R_{BB} ; panel (c): R_W . Real part (thin solid red), imaginary part (dashed blue), modulus (thick black).

Thus, the modified RM spread function $R_{BB}(\phi)$ has a vanishing imaginary part and a real part, which reproduces the shape of the envelope of the function $R(\phi)$ (Fig. 1b).

Another way to improve the RM spread function follows from Frick et al. (2010). Their algorithm uses the symmetry argument (the results of Sect. 5 give strong support for this argument - realistic objects mainly look like even objects in Faraday depth space). It means that if the object is centered at Faraday depth ϕ_0 , then $F(2\phi_0 - \phi) = F(\phi)$. In λ^2 space this gives

$$P(-\lambda^2) = \exp(-4i\phi_0\lambda^2)P(\lambda^2), \quad (15)$$

which means in terms of the spread function for a single window

$$R_W(\phi) = 2K \frac{\sin(\phi\Delta\lambda^2)}{\phi} \cos(2\phi\lambda_0^2) \quad (16)$$

and

$$\tilde{F}(\phi) = e^{-4i\phi_0\lambda_0^2} F(\phi) * R_W(\phi). \quad (17)$$

The RM spread function $R_W(\phi)$ is also shown in Fig. 1c. Similar to R_{BB} this function has no imaginary part, but the real part remains exactly the same as in Eq. (12), compare thin solid lines in Fig. 1a and Fig. 1c.

Note that the symmetry assumption used here works straightforward only if there is only one source along the light of sight. If there are several sources the assumption should be applied using the wavelet technique.

4 CLEANING AND WAVELETS

We discussed above the reconstruction of objects symmetric in Faraday space around $\phi = \phi_0$. The simplest objects for recognition are point-like sources, which can be described in Faraday space by delta functions

$$F(\phi) = F_0 e^{2i\chi_0} \delta(\phi - \phi_0). \quad (18)$$

The corresponding polarized intensity is given by

$$P(\lambda^2) = F_0 e^{2i\chi_0} e^{2i\phi_0\lambda^2}. \quad (19)$$

Note that the relation (19) determines $P(\lambda^2)$ for $\lambda^2 < 0$ and it follows the symmetry property (15) which is the starting point for our approach. It means that the traditional RM Synthesis for a point-like source indirectly implies this symmetry argument and can be considered as a particular case of the method presented in this paper.

To recognize several point-like sources located on the same line of sight one can apply a deconvolution procedure using the Faraday dispersion function, called “RM-CLEAN” (Heald 2009). This procedure iteratively finds the maximum in the reconstructed Faraday dispersion function and then iteratively subtracts the scaled versions of the RMSF until the noise level is reached, after which a smoothed representation of the “CLEAN model” is used as the approximate true Faraday dispersion function.

After removing the brightest structure (including the corresponding sidelobes) the procedure finds the maximum in the remaining data and restarts the iteration. Heald et al. (2009) showed how well RM-CLEAN deconvolved RM cubes from the WSRT SINGS survey.

Let us show how this cleaning of objects, compact in Faraday depth space, can be realized in terms of wavelet-based RM Synthesis. We use the example, presented in Fig. 3 from Heald (2009). This figure is partially reproduced in our Fig. 2, where the observed $U(\lambda^2)$ and $Q(\lambda^2)$, the restored $F(\phi)$ before and after cleaning and the polarization angles observed and reconstructed after cleaning are shown. The observations are done in two windows. In Fig. 3a we show the modulus of the wavelet coefficients $|w_+|$, calculated from same observed $U(\lambda^2)$ and $Q(\lambda^2)$. Then using the symmetry argument for the main maximum we find $|w_-|$ and reconstruct $F(\phi)$. Taking the dominating maximum in $F(\phi)$ at $\phi = \phi_0 = -185$ rad m⁻² we replace it by an equivalent point source and calculate for this point source the wavelet transform w_1 , based on the same sample of observational channels as in original data. Then we subtract w_1 from the wavelet transform w of original data and we obtain the wavelet image, shown in the second panel of Fig. 3b, which demonstrates a dominating maximum at $\phi = 165$ rad m⁻². Using again the symmetry argument we get w_- and restore the second point-like source in $F(\phi)$. The corresponding polarization angles, calculated for the given observational windows are shown in the panel (c), which is practically equivalent to the result of RM-CLEAN (Fig. 2). Summarizing this section, we conclude that, in contrast to the extended sources, for a source that is point-like in Faraday space, wavelet-based RM Synthesis gives just the same result as conventional RM Synthesis.

5 GALACTIC MAGNETIC FIELD IN FARADAY DEPTH SPACE

The complex-valued intensity of polarized radio emission for a given wavelength is

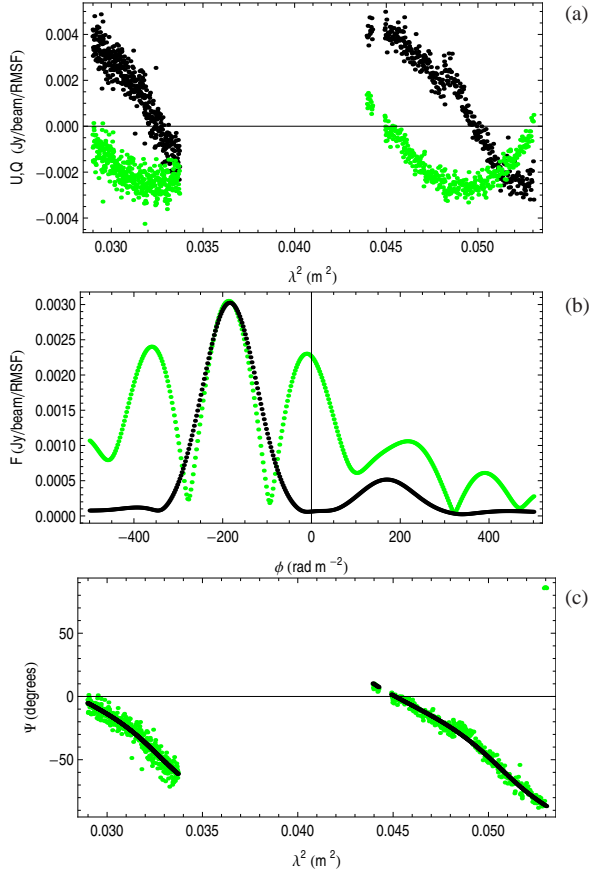


Figure 2. Example of the RM-CLEAN process from Heald (2009) for a bright point source in the field of the galaxy NGC 7331. Panel (a): observed Q (black) and U (green); panel (b): the restored $F(\phi)$ before cleaning (green) and after cleaning (black); panel (c): observed polarization angles (green) and reconstructed after cleaning (black).

$$P(\lambda^2) = \int_0^\infty \varepsilon(x) e^{2i\chi(x)} e^{2i\phi(x)\lambda^2} dx, \quad (20)$$

defined by the emissivity ε and the intrinsic polarization angle χ along the line of sight. The integral is taken over the whole emitting region. The emissivity depends on the relativistic (cosmic-ray) electron density n_c , the magnetic field component perpendicular to the line of sight and the synchrotron spectral index α (assuming $\alpha = 0.9$ below) as (e.g. Ginzburg & Syrovatskii (1965))

$$\varepsilon(x) = n_c(x) |B_\perp(x)|^{1+\alpha}. \quad (21)$$

Our analysis starts from an investigation of the typical shapes of the Faraday dispersion functions expected for lines of sight crossing galactic discs with several simple distributions of the parallel magnetic field, which provides the Faraday rotation. These distributions are shown in Fig. 4a. We consider two symmetric distributions with respect to center at $x = x_0$. The first one has a sharp boundary at $x = x_0 \pm h$,

$$B_{1\parallel}(x) = \begin{cases} a_1, & |x - x_0| \leq h \\ 0, & |x - x_0| > h \end{cases}. \quad (22)$$

Here x_0 is position of galactic equatorial plane and h is the half thickness of the galactic disc. The second distribution has a smooth shape approximated by a Gaussian function with the scale height h ,

$$B_{2\parallel}(x) = a_2 e^{-(x-x_0)^2/h^2}. \quad (23)$$

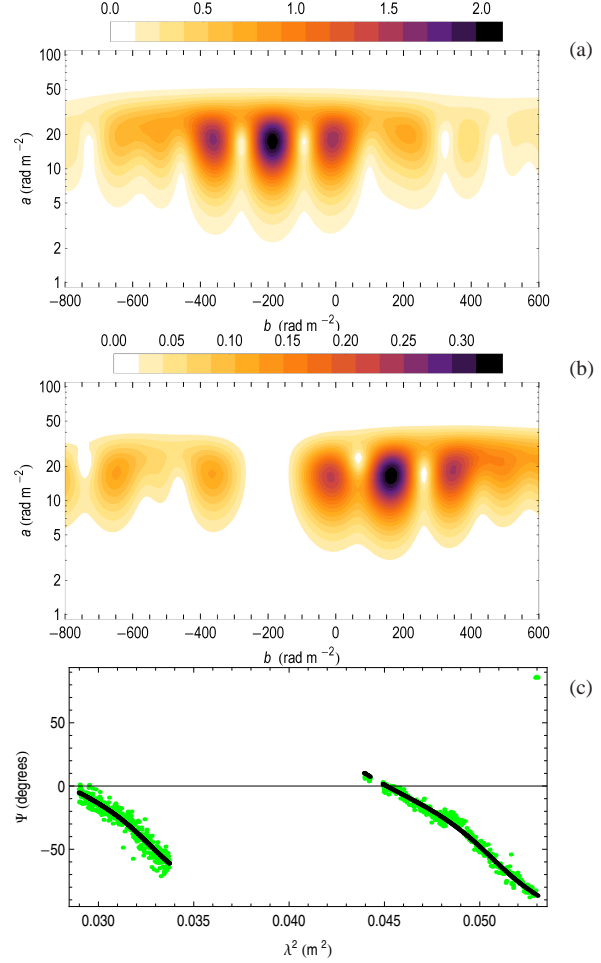


Figure 3. Wavelet cleaning for the same example as in Fig. 2. Panel (a): wavelet plane after the first step (the symmetry of the main maximum is used); panel (b): wavelet plane after cleaning of the first point source and using symmetry argument for the rest (note that the amplitudes in the two figures are different); panel (c): observed polarization angles (green) and reconstructed after two-step wavelet cleaning (black). Here and below colors are given in a relative scale specific for each panel and black color corresponds to maximum.

For comparison we take into consideration a distribution with a field reversal along the line of sight

$$B_{3\parallel}(x) = -a_3 \frac{(x - x_0)}{h} e^{-(x-x_0)^2/h^2}. \quad (24)$$

The amplitudes a_2 and a_3 are adjusted to obtain the same maximal Faraday depth for all three distributions. We choose an amplitude of the magnetic field of $a_1 = 2 \mu\text{G}$ and $h = 0.5 \text{ kpc}$. The densities of relativistic electrons n_c (responsible for synchrotron emission) and thermal electrons n_e (responsible for Faraday rotation) measured in cm^{-3} are assumed to have Gaussian profiles

$$n_c(x) = C e^{-(x-x_0)^2/h_c^2}, \quad n_e(x) = 0.03 e^{-(x-x_0)^2/h_e^2}. \quad (25)$$

Here C (measured in cm^{-3}) is the relativistic electron density at the galactic midplane. We assume that the scale height of the relativistic electrons h_c is twice that of the thermal electrons h_e and that the scale height of the magnetic field h is the same as that of the thermal electrons h_e . We use C as a normalization constant for F and P , so that they are numerically evaluated in arbitrary but mutually consistent units. Fig. 4b shows that the symmetric profiles

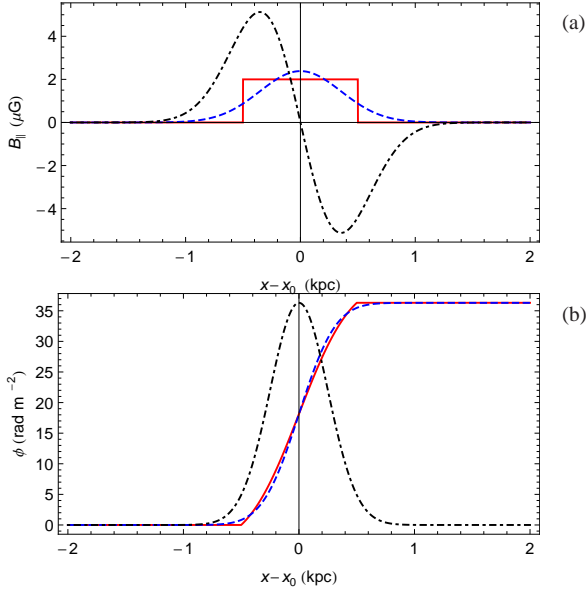


Figure 4. Typical shapes of magnetic field distribution. Panel (a): B_1 (solid line, red), B_2 (dashed, blue), B_3 (dot-dashed, black); panel (b): corresponding Faraday depths ϕ .

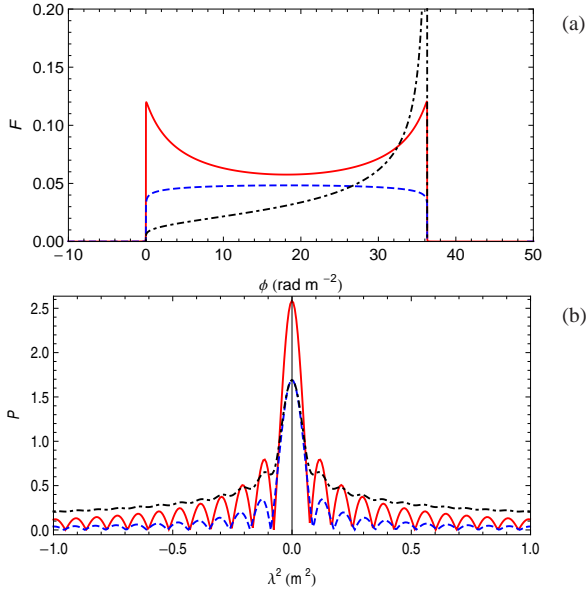


Figure 5. Real part of the Faraday dispersion function $F(\phi)$ (panel a), $\text{Im } F = 0$, and the modulus of corresponding $P(\lambda^2)$ (panel b) for different magnetic field profiles: B_1 (solid line, red), B_2 (dashed, blue), B_3 (dot-dashed, black).

of the parallel magnetic field (first two cases) lead to a monotonic increase (decrease) of Faraday depth along the coordinate x inside the galaxy, while the antisymmetric profile (last case) leads to an inversion - the central galactic plane becomes the most distant (or most nearby) point in Faraday depth space.

For the sake of normalization we choose the direction of the perpendicular field to obtain a purely real P (i.e. zero polarization angle). The perpendicular component is described by the same distributions as for the parallel component in Eqs. (22)-(24). Namely, we take $B_{1\perp} = B_{1\parallel}$, $B_{2\perp} = B_{2\parallel}$ and $B_{3\perp} = B_{2\parallel}$.

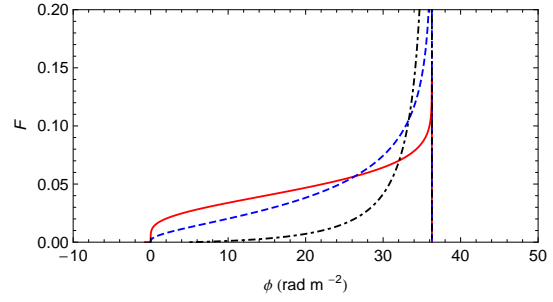


Figure 6. Faraday dispersion function $F(\phi)$ for different separations Δx between the regions of synchrotron emission and Faraday rotation with Gaussian profiles: $\Delta x = 0.1$ kpc (solid line, red), $\Delta x = 0.2$ kpc (dashed, blue), $\Delta x = 0.5$ kpc (dot-dashed, black).

Fig. 5a shows that both even profiles (B_1 and B_2) produce in Faraday space basically box-like distributions with sharp boundaries. In contrast, Faraday depth in the case of the magnetic field with a reversal varies slowly near the point where Faraday depth becomes minimal and has a sharp point-like structure in $F(\phi)$ near the point where ϕ is maximal while F is still nonvanishing, in the given examples F is even maximal at this point.

We conclude from Fig. 5a that box-like and point-like shapes of $F(\phi)$ are common in simple models of disc components of spiral galaxies. Of course, one can obtain a smoother distribution of $F(\phi)$ by taking a wider distribution for thermal electrons than for relativistic ones. According to Fig. 5b the level of polarized intensity at large λ^2 is higher for pointed F profiles (hence easier to recognize by low-frequency observations) than for box-like ones.

In general, the synchrotron emission is not necessarily located in the same region as the Faraday rotation. This leads to a so-called “Faraday screen” which can be due to a specific magnetic field configuration (strong B_{\parallel} , weak B_{\perp}) or to a difference between distributions of $n_e(x)$ and $n_e(x)$. For simplicity, we shift $\varepsilon(x)$ by some distance Δx . The resulting Faraday dispersion functions for Gaussian shape (the case B_2 in Fig. 4) and different Faraday screen separations are shown in Fig. 6. For larger values of Δx the Faraday dispersion function F becomes more pointed and asymmetric.

6 THE ROLE OF THE SPECTRAL RANGE

The efficiency of RM Synthesis crucially depends on the observational range $\lambda_{\min} < \lambda < \lambda_{\max}$ (Brentjens & de Bruyn 2005). Wavelets give a helpful illustration for the role of these parameters.

Fig. 7 shows the wavelet planes for the first artificial example (solid lines in Fig. 5), calculated for different observational windows. Each panel shows the absolute value of the wavelet coefficient $W(a, b)$ in the (a, b) plane. The horizontal axis (b) presents the position in Faraday depth space, the vertical axis gives the scale a in logarithmic presentation. The upper bound is first fixed at $\lambda_{\max} = 2.5$ m. The panel (a) shows the wavelet plane simulated for the lower bound $\lambda_{\min} = 6$ cm (thus $0.0036 < \lambda^2 < 6.25$ m^2). The large horizontal dark feature at $a \approx 40$ rad m^{-2} corresponds to the box-like structure, and the two tapering structures are generated by the sharp borders of this box. The next panel shows what remains in the wavelet plane if the lower bound is moved to $\lambda_{\min} = 21$ cm (the window $0.044 < \lambda^2 < 6.25$ m^2). The central spot (responsible for the box) is almost completely lost even at these relatively short wavelengths. Applying the actual LOFAR highband window ($1.56 < \lambda^2 < 6.25$ m^2), only weak traces of side

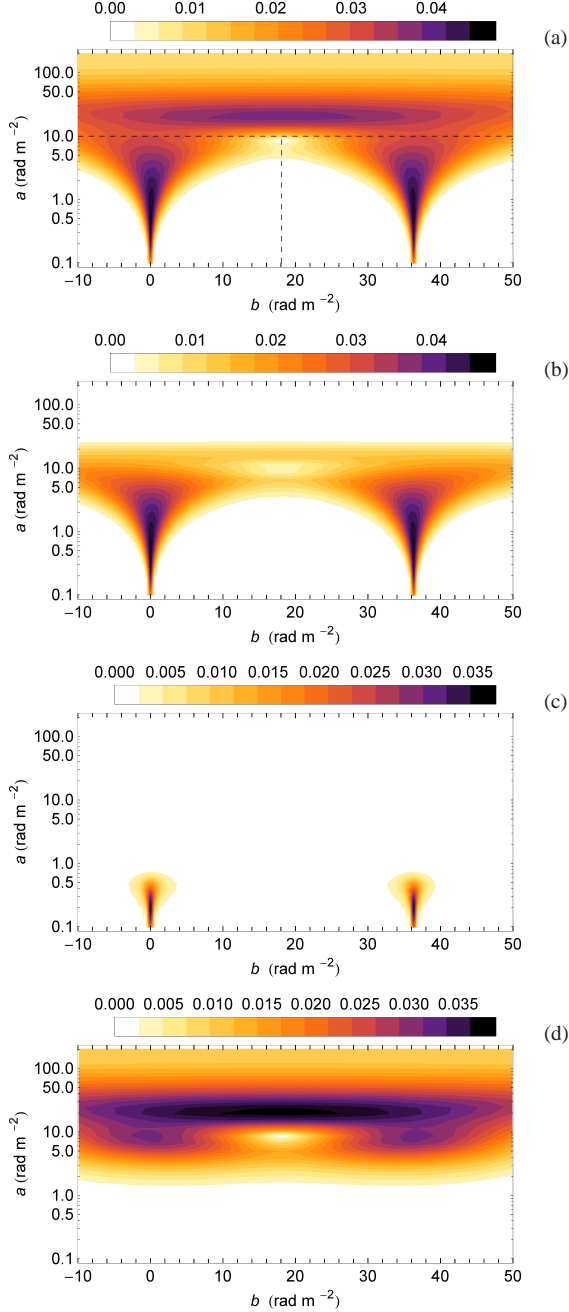


Figure 7. Wavelet plane $|w_F(a, b)|$ of the example of Figs. 4 and 5 (solid lines) for various spectral windows. Panel (a): $0.06 < \lambda < 2.5$ m; panel (b): $0.21 < \lambda < 2.5$ m; panel (c): $1.25 < \lambda < 2.5$ m; panel (d): $0.06 < \lambda < 0.21$ m.

horns remain in the wavelet plane (panel c). The lower panel (d) in Fig. 7 shows the wavelet plane for a relatively high-frequency window ($0.06 < \lambda < 0.21$ m), which perfectly keeps all information concerning the large scales, but completely loses any information concerning the small scales, responsible in this example for the abrupt boundaries.

For applying the symmetry argument expressed by Eq. (8) the position of each local maximum ϕ_0 and the domain of its influence should be defined. In Fig. 7a we recognize three maxima and we divide the wavelet plane in three parts: one domain corresponds

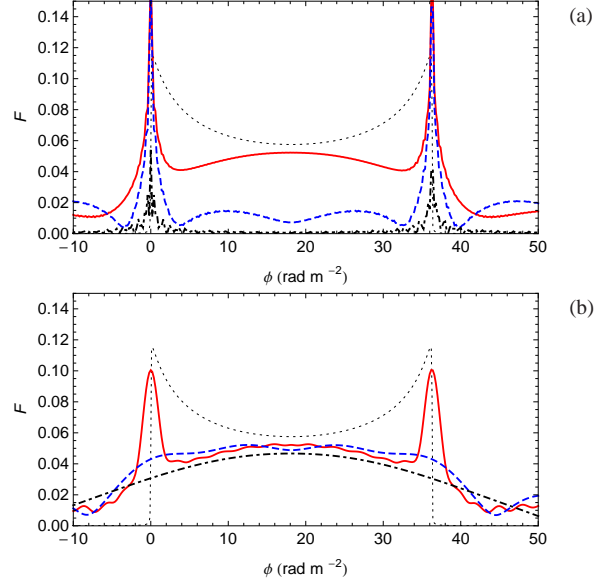


Figure 8. Test Faraday dispersion function (black dots in both panels), the same as shown in Fig. 5a (solid red line), and results of RM Synthesis performed from the wavelet planes shown in Fig. 7 for various spectral windows. Panel (a): $0.06 < \lambda < 2.5$ m (solid, red line), $0.21 < \lambda < 2.5$ m (dashed, blue), $1.25 < \lambda < 2.5$ m (dash-dot, black); panel (b): $0.06 < \lambda < 1.0$ m (solid, red line), $0.06 < \lambda < 0.42$ m (dashed, blue), $0.06 < \lambda < 0.21$ m (dash-dot, black).

$a > 10$ rad m⁻² and two domains for $a \leq 10$ rad m⁻² are separated at $b \approx 18$ rad m⁻². Separatrices are shown in Fig. 7a by dashed lines. In the case shown in Fig. 7c only two lower domains can be recognized. Note, that two horns-like structures are associated with the sharp borders, which are not symmetric objects, and the application of the symmetry assumption to them does not improve the reconstruction.

Fig. 8 shows how the shrinking of the wavelength range of observations reduces the quality of the Faraday function reconstructed from the corresponding sets of $w_F(a, b)$. We see that increasing of λ_{\min} leads to a gradual decay of the reconstructed F in the main bulk of the structure (Fig. 8a). Starting from $\lambda_{\min} = 21$ cm we reconstruct details associated with the boundaries only. Decreasing the upper bound λ_{\max} we lose the small-scale details, restoring a smooth structure only (Fig. 8b).

The possibility to reconstruct a structure of scale $\Delta\phi$ in Faraday space is determined by the quantity $X = \Delta\phi \lambda^2$ where λ is the wavelength at which the observations are performed. We illustrate the role of this quantity for the large-scale structure from Fig. 8a. The relevant parameters here are $\Delta\phi = 38$ rad m⁻² and $\lambda = \lambda_{\min}$. $X = 1.68$ is for the dashed (blue) line and $X = 60$ for the dash-dot (black) lines. Because the latter curve keeps the information of sharp ends of the distribution $F(\phi)$ and even the first curve loses a substantial part of the signal,

$$X = \Delta\phi \lambda_{\min}^2 \lesssim 1 \quad (26)$$

is the condition to observe a galaxy as an extended source in Faraday space rather than as a couple of point-like sources (Brentjens & de Bruyn 2005). For observations in the LOFAR highband ($\lambda_{\min} = 1.25$ m) this gives $\Delta\phi = 0.64$ rad m⁻², which is at least one order of magnitude lower than a typical value for contemporary galaxies. If $\lambda_{\min} = 0.167$ m (by including observations e.g.

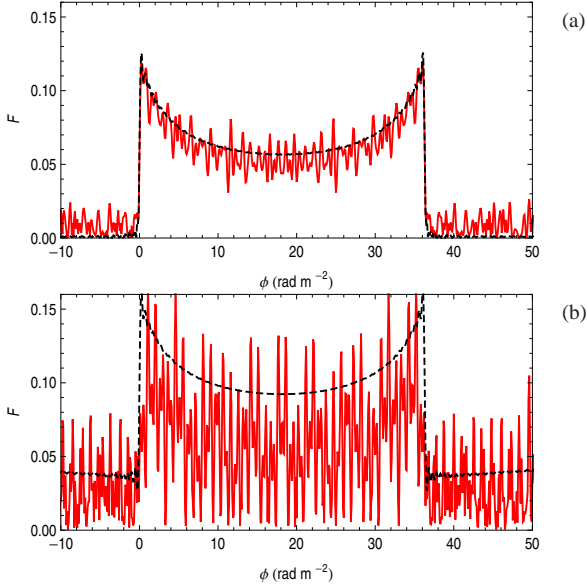


Figure 9. Modulus of the Faraday dispersion function F obtained from wavelet-based RM Synthesis performed for the observational window $0.06 < \lambda < 2.5$ m with 1024 (panel a) and 128 (panel b) channels providing uniform sampling in λ^2 space (dashed black line) or uniform sampling in frequency space (solid red line).

with the ASKAP telescope) this yields a much more comfortable $\Delta\phi = 35 \text{ rad m}^{-2}$.

For distant galaxies the wavelength in the framework of the source is $\lambda/(1+z)$ (z is the redshift) and Eq. (26) reads

$$X = \Delta\phi \lambda_{\min}^2 / (1+z)^2 \lesssim 1. \quad (27)$$

Taking $Z = 3$ one obtains that $\Delta\phi \approx 10 \text{ rad m}^{-2}$ for LOFAR-type observations. LOFAR observations can also be used to isolate a contribution of weak intergalactic magnetic fields, which can give typical $\Delta\phi$ much lower than that for galactic magnetic fields.

As we conclude above, RM Synthesis of extended magnetic configurations requires a proper wavelength range of observations. λ_{\min} has to be small enough to reproduce the grand design of F and a large λ_{\max} is required to reproduce sharp details of F . Obviously, RM Synthesis demands a substantial number of channels in the observational range to perform the Fourier transform included in the method. A dispersion function F which is extended over a large range of Faraday depths requires a large number of channels. If the number of channels is limited, the main question is how to distribute the channels between the given values of λ_{\min} and λ_{\max} . We clarify this using the example considered for Fig. 7. For the sake of the definiteness we compare two samplings, i.e. a uniform spacing in frequency space and that one in the λ^2 space.

We presume that the spectral range of observations is sufficiently large and use $\lambda_{\min} = 6 \text{ cm}$ and $\lambda_{\max} = 2.5 \text{ m}$ and apply the wavelet-based RM Synthesis. Fig. 9a presents the results for a large (1024) number of channels. We see that even here a uniform spacing in λ^2 looks better than one in frequency space, which gives a more noisy result. The difference between the two kinds of spacings becomes much more pronounced for a moderate (128) number of channels. The results for the uniform spacing in λ^2 is more or less similar to that one in the upper panel, while for a uniform spacing in frequency the noise in F becomes comparable to the signal. It is clear that the effect is essential for large spectral windows (namely, for a large ratio $\lambda_{\max}/\lambda_{\min}$) because a uniform

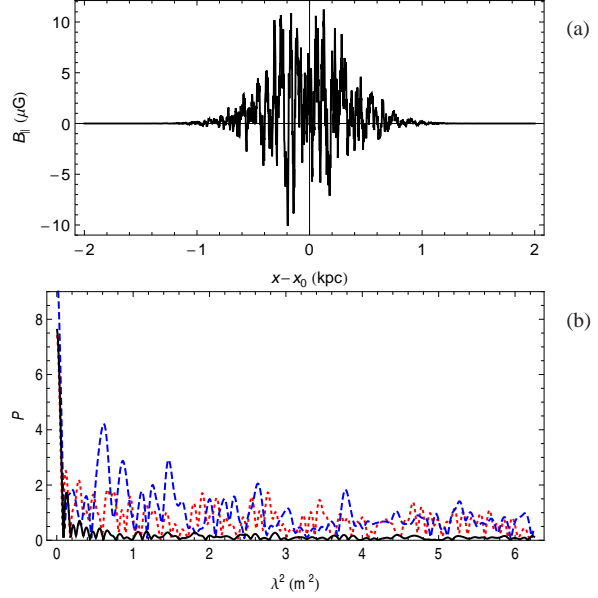


Figure 10. Magnetic field distributions over a galactic disc. The ratio of small-scale (b) and large-scale (B) components is $b/B = 2$, the ratio of spatial scales of the components is $l/2h = 0.1$. Panel (a): light-of-sight magnetic field; panel (b): polarized intensity. The long and short dashed lines give P for two different realizations of the turbulent magnetic fields calculated for a very narrow beam, while the solid line shows P calculated for a beam which contains 50 independent turbulent cells.

spacing in frequency leads to points crowding at small λ^2 . A poor sampling at large λ^2 (essential to detect small scales in Faraday depth space) results in small-scale noise in the reconstructed signal. Note that the advantages of uniform spacing in λ^2 was first discussed by Ruzmaikin & Sokoloff (1979).

7 SMALL-SCALE MAGNETIC FIELDS

In contrast to the traditional methods, wavelet-based RM Synthesis opens a new option to quantify the small-scale (turbulent) component of magnetic field. Remember that it is widely believed that one can isolate two contributions in total magnetic field, i.e. the large-scale (regular) magnetic field and the small-scale one. Correspondingly, the Faraday dispersion function F and the Faraday depth ϕ have two corresponding components, coming from large-scale and turbulent fields. The traditional Burn (1966) theory suggests that averaging P over turbulent variations yields an additional depolarization term like internal Faraday dispersion and beam depolarization. In principle, one could try to modify Eq. (1) to isolate the large-scale contribution and parameterize the small-scale one by intrinsic Faraday dispersion and beam depolarization. Wavelets allow us to perform this procedure in a more straightforward way and to obtain more detailed information concerning the small-scale component.

We start here with an example of a magnetic field which contains large-scale and turbulent components (Fig. 10a) and consider a slab with thickness $2h = 1 \text{ kpc}$ with a large-scale magnetic field B and a turbulent magnetic field with a Kolmogorov spectrum and an rms value b with the scale $l = 0.1 \text{ kpc}$ ($l/2h = 1/20$) and $b/B = 2$. The polarized intensity obtained from such a slab is affected by two depolarization effects. One effect known as internal Faraday dispersion occurs because several (about 20 in our example) inde-

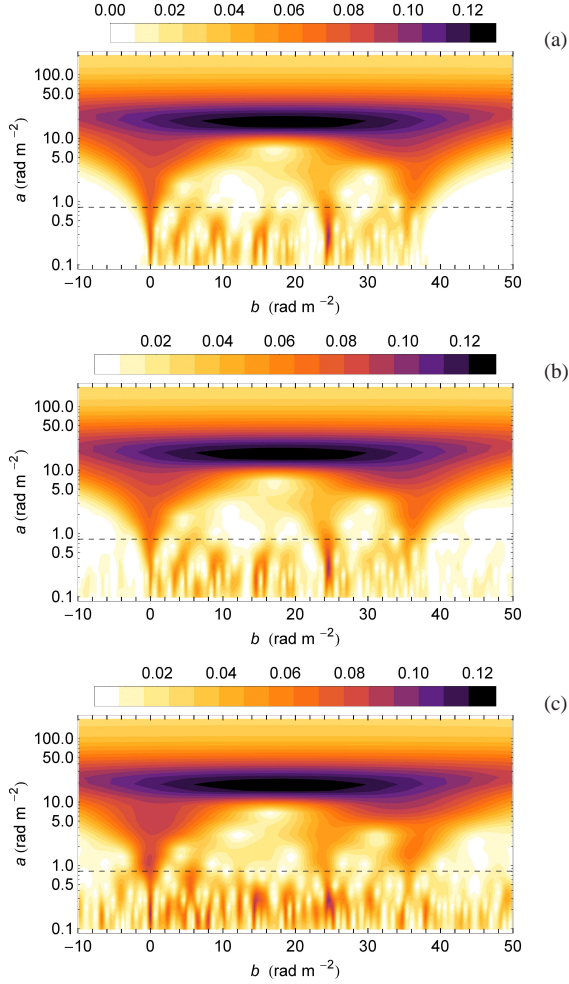


Figure 11. Wavelet plane $w_F(a, b)$ calculated for different ratios of signal-to-noise from $P(\lambda^2)$, obtained for the wide beam (shown in Fig. 10b by the black line). From top to bottom: signal without noise, signal-to-noise ratios of 2 and 0.5. The horizontal dashed line shows the upper bound of the domain admissible to LOFAR-type observations.

pendent turbulent cells are located at a given line of sight passing through the slab. This effect occurs even for a very narrow beam, with a cross-section with the slab surface containing just one turbulent cell. The corresponding P for two independent realizations of the turbulent field is shown by dashed lines in Fig. 10b.

The other depolarization effect arises because the beam is usually wide enough to contain many turbulent cells. If, say, the beam diameter on the slab is 1 kpc it contains about 100 independent cells. The polarized emission passing through independent cells contributes to P , leading to additional depolarization known as beam depolarization. The values of P calculated for a beam with a cross-section containing 50 independent cells is shown by the solid line in Fig. 10b. We see that typical P/P_{\max} values are only a few percent for large λ^2 . One could conclude that the emission is almost completely depolarized and useless for RM Synthesis. However, the wavelet method being applied to P shows a well-ordered structure (Fig. 11). The point is that wavelets separate contributions from different spatial scales and associate them with specific domains in the plot.

In Fig. 11a, we see a contribution from the large-scale magnetic field (the long horizontal feature at the upper part of the panel)

and various small-scale details at the bottom which represent the contributions of individual turbulent cells. Having a limited spectral range covered by the observations, we can obtain wavelet coefficients in a limited part of the wavelet plane only. The border of this part is given by Eq. (26) which reads as

$$a_{\max} = \lambda_{\min}^{-2}. \quad (28)$$

Here we take into account that for structures of size a the range of Faraday depth is of order $\Delta\phi = a^{-1}$. The upper limit of the domain admissible for LOFAR observations is shown in Fig. 11 by a horizontal dashed line. We conclude that the contribution of the large-scale magnetic field remains inaccessible for this type of observations while the small-scale details remain visible. Note that the wavelet transform presented in the figure allows us to recognize the range of Faraday depths in which small-scale structures occur (from 0 rad m⁻² to 38 rad m⁻² for the given example). Obviously, using data at large λ^2 only, we cannot confirm (or reject) the existence of a large-scale magnetic field.

The method under discussion presumes that the signal-to-noise ratio is sufficiently large. The lower panels of Fig. 11b present the result of the wavelet RM Synthesis for P for which random instrumental noise (independent in each spectral channel from the noise in the other channels) is added. The signal-to-noise ratio (calculated from the averaged signal and the noise per frequency channel and per Q and U point for the observational range $1.25 < \lambda < 2.5$ m) is about 2 (panel b) and the contribution of the small-scale fields is easily distinguishable from instrumental noise. These plots show that a signal-to-noise ratio about 2 (per channel and per Q and U point) or higher is sufficient to isolate the range in Faraday space responsible for the small-scale magnetic fields. For illustrative purposes we give an example with the signal-to-noise ratio of about 0.5 and demonstrate that the contribution of small-scale field cannot be distinguished from instrumental noise (Fig. 11c).

8 A SYNTHETIC EXAMPLE

To summarize our findings and to conclude what can be learned from polarized radio observations of galactic magnetic fields using different RM Synthesis techniques, we now consider a complex test example. Suppose that we observe a galaxy which hosts both regular and turbulent magnetic fields (like the example considered in Sect. 7) and a strong point-like source of polarized radio emission behind the galaxy on the same line of sight. Independent of its position in physical space (coordinate x) behind the galaxy, this source appears in Faraday space like attached to the galactic backside. For sake of definiteness we suppose that the contribution to F which comes from the galaxy is purely real and that one from the point source is purely imaginary. The task for the analysis is to reconstruct the Faraday dispersion model and then to restore the intensity and the polarization angle of the point source, to separate the contribution of large-scale and small-scale galactic magnetic field and recognize the shape of the large-scale structure.

Fig. 12a shows the wavelet plane calculated for this signal. We recognize here an extended structure in the region of large scales, $10 \lesssim a \lesssim 50$ rad m⁻², which we identify with the contribution of a galactic disc as a whole, small-scale details at $a < 1$ rad m⁻², which we identify as the contributions of the small-scale magnetic fields, and a bright horn located at $b \approx 37$ rad m⁻². Then we perform the wavelet-based RM Synthesis using the symmetry arguments to the galactic contribution with the reflection point at $\phi_0^g = 18$ rad m⁻² and considering the domain of the horn as a point-like source, i.e.

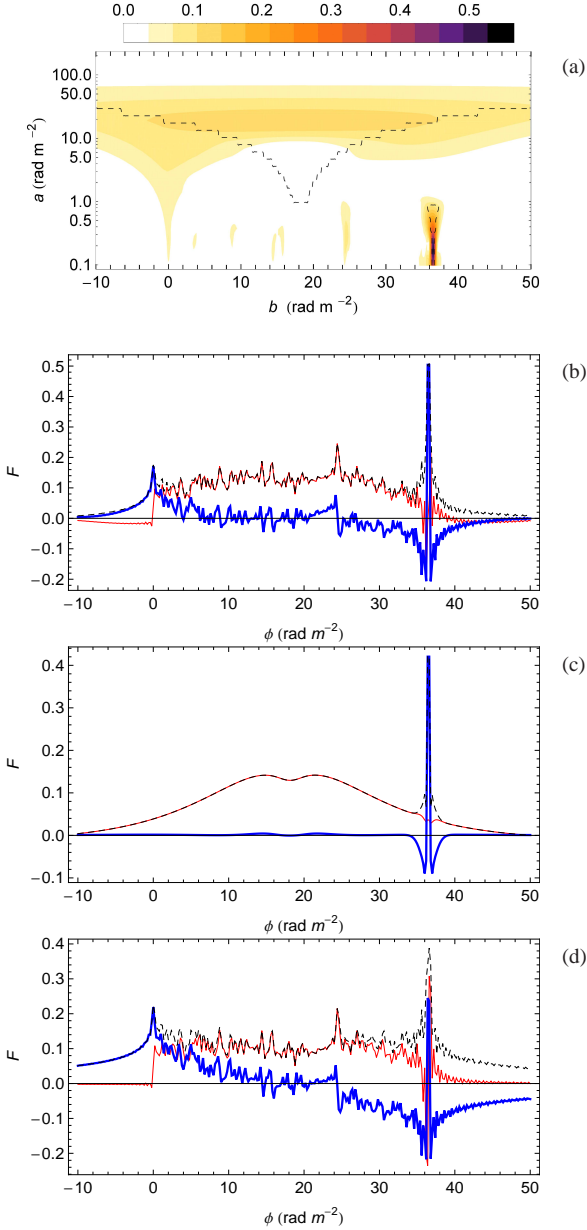


Figure 12. Panel (a): Wavelet plane $w_F(a, b)$ (in colors online) calculated from the polarized radio emission $P(\lambda^2)$ generated by turbulent galactic magnetic fields superimposed on a point source behind the galaxy. The results of RM Synthesis are shown in panels (b)–(d). Panel (b): wavelet reconstruction using the whole wavelet plane; panel (c): wavelet reconstruction using only the domains marked in the wavelet plane by dashed lines in panel (a); panel (d): reconstruction by standard RM Synthesis. The red thin line is for the real part, the blue thick line for the imaginary part, and the black dashed line for the modulus.

apply the symmetry condition at the point $\phi_0^h = 37 \text{ rad m}^{-2}$. This means

$$\phi_0(a, b) = \begin{cases} \phi_0^g, & a > 1 \\ \phi_0^h, & a \leq 1 \end{cases} \quad (29)$$

Applying the symmetry arguments for the whole domain would amplify the small-scale noise and reflect it with respect to the position of the maximum. Therefore we perform a reflection locally

(only in vicinity of the maxima) which leads to the definition

$$w_-(a, b) = \begin{cases} w_+(a, 2\phi_0(a, b) - b), & |b - \phi_0(a, b)| \leq a \\ 0, & |b - \phi_0(a, b)| > a \end{cases} \quad (30)$$

instead of Eq. (8). The dashed lines in Fig. 12a shows two domains around each maxima in which the symmetry arguments are used for calculation of w_- following Eqs. (29–30).

The reconstruction in Fig. 12b shows a point-like source and a smooth contribution from the large-scale magnetic field, superimposed onto fluctuations associated with the small-scale fields. If we are not interested in the small-scale details we ignore the wavelet coefficients outside isolated domains and obtain a smoothed F which represents the contribution of the mean field in the disc and the point-like source only (Fig. 12c). We see a smoothed real contribution from the mean field and an imaginary point-like source, i.e. the method correctly reproduces the polarization angles. For comparison with Fig. 12b, we show in Fig. 12d the result obtained by the standard RM Synthesis technique where the phase information is completely lost. More specifically, the blue thick line at Fig. 12b follows the horizontal axis as required by the model while a negative trend of the blue thick line is visible in Fig. 12d.

9 DISCUSSION AND CONCLUSIONS

We considered how to apply RM Synthesis to extract information concerning magnetic fields of spiral galaxies from polarized emission data. The main attention was given to two related novelties in the method, i.e. the symmetry argument and the wavelet technique. Symmetry arguments open the possibility to reconstruct $P(\lambda^2)$ for negative λ^2 from $P(\lambda^2)$ for positive λ^2 . If F contains several contributions (say, the disc and an unresolved source) the reconstruction can be performed locally in Faraday depth space using wavelets. The wavelet technique appears to be useful in RM Synthesis in several areas which are not directly related to the problem of negative λ^2 . In particular, they allow us to perform RM Synthesis locally in Faraday depth space.

The idea of RM Synthesis was applied first for sources which are presumed to be point-like in Faraday space or a combination of several point-like sources (Haverkorn et al. 2003; de Bruyn & Brentjens 2005; Heald et al. 2009; Wolleben et al. 2010; Landecker et al. 2010). We demonstrated that the traditional RM Synthesis for a point-like source indirectly implies a symmetry argument (see Eq. 22) and, in this sense, can be considered as a particular case of the method under discussion here.

Investigating the applications of RM Synthesis to the polarization details associated with small-scale magnetic fields, we isolated an option which was not covered by Burn (1966). Burn (1966) (see also Sokoloff et al. (1998)) described a contribution of small-scale fields in terms of Faraday dispersion and beam depolarization, i.e. using averages over a corresponding statistical ensemble. Here we use the complex polarization P for RM Synthesis without any averaging and demonstrate that it allows us to obtain (if the λ^2 coverage is adequate) a range in Faraday space where the contribution from small-scale field is located.

A general conclusion concerning the applicability of RM Synthesis to the interpretation of the radio polarization data for extended sources like spiral galaxies is that quite severe requirements are needed to provide the full applicability of the method. The most severe one is the requirement for the wavelength range where short wavelengths are highly desired. Brown et al. (2009) show that RM Synthesis applied at the border of its applicability (say, if the num-

ber of frequency channels is very small) can sometimes be misleading.

Traditional methods of the pattern recognition for magnetic structures in spiral galaxies (e.g. Ruzmaikin et al. (1990); Sokoloff et al. (1992); Frick et al. (2000); Fletcher et al. (2004); Patrikeev et al. (2006); Stepanov et al. (2008)) were mainly based on the interpretation of polarization angles at a few wavelengths only. The efforts of the above papers concentrated mainly on the distribution of polarization angles in the radio image. Modern wide-band observations with many frequency channels and RM Synthesis open wide perspectives to extract much more information from the polarization signal in a given telescope beam. However, they cannot fully replace the traditional analysis of the distribution of the polarization patterns. Of course, the development of RM Synthesis in order to deal with radio images as a whole rather than with just one beam is a goal for further developments, and wavelets are likely to be helpful here. However, this is outside of the scope of this paper.

Obviously, a quantified characteristic of reconstruction fidelity of the algorithm under discussion is highly desirable. However, a general norm is not informative in a spectral problems with varying windows - one can completely lose the large-scale structures and reconstruct precisely the small-scale details (or vice versa). Fig. 8 is a good illustration for that: the central part of the structure is completely lost (for $0.06 < \lambda < 0.42$), but the borders are reconstructed quite well. Thus the "global fidelity" is very poor, while the "fidelity of border reconstruction" is fine. So, we avoided intentionally to quantify the quality of the reconstruction by a norm in some functional space.

The RM Synthesis approach was suggested in the context of observations with a rather large value of λ_{\min} while the traditional method to measure RMs between only two wide frequency bands intensively used the data at $\lambda = 3$ cm and $\lambda = 6$ cm and rarely used the wavelength range $\lambda > 22$ cm. The attention of the traditional method was focused on the magnetic field configuration rather than on the Faraday dispersion function which appears in this context as an intermediate rather than a final result. On the other hand, observations in the wavelength range $1.25 < \lambda < 2.5$ m (the LOFAR high band) cannot recognize a lot of structures which would be accessible to observations in the wavelength range $0.03 < \lambda < 2.5$ m with an adequate coverage. However, this option will have to wait for future radio telescopes like the SKA.

This paper, although based on model examples, presents an optimistic view that the combination the ideas of traditional RM studies of galactic magnetic fields at short wavelengths and those of RM Synthesis at large wavelengths is possible. The final conclusion can be made after application to real data.

ACKNOWLEDGEMENTS

This work was supported by the DFG-RFBR grant 436RUS113/969 (08-02-92881) and by the Council of the President of the Russian Federation (grant MD-4471.2011.1). We thank Dr. George Heald for providing observational data and for useful discussions. Our special thanks go to our referee, Dr. Michiel Brentjens, for his efforts to improve the paper.

REFERENCES

- Brown S., Rudnick L., Farnsworth D., 2009, in IAU Symposium Vol. 259 of IAU Symposium, Detecting magnetic fields in large-scale structure with radio polarization. pp 669–670
- Burn B. J., 1966, MNRAS, 133, 67
- de Bruyn A. G., Brentjens M. A., 2005, A&A, 441, 931
- Fletcher A., Berkuijsen E. M., Beck R., Shukurov A., 2004, A&A, 414, 53
- Frick P., Beck R., Shukurov A., Sokoloff D., Ehle M., Kamphuis J., 2000, MNRAS, 318, 925
- Frick P., Sokoloff D., Stepanov R., Beck R., 2010, MNRAS, 401, L24
- Ginzburg V. L., Syrovatskii S. I., 1965, Ann. Rev. Astron. Astrophys., 3, 297
- Haverkorn M., Katgert P., de Bruyn A. G., 2003, A&A, 403, 1031
- Heald G., 2009, in IAU Symposium Vol. 259 of IAU Symposium, The Faraday rotation measure synthesis technique. pp 591–602
- Heald G., Braun R., Edmonds R., 2009, A&A, 503, 409
- Landecker T. L., Reich W., Reid R. I., Reich P., Wolleben M., Kothes R., Uyaniker B., Gray A. D., Del Rizzo D., Fürst E., Taylor A. R., Wielebinski R., 2010, A&A, 520, A80+
- Patrikeev I., Fletcher A., Stepanov R., Beck R., Berkuijsen E. M., Frick P., Horellou C., 2006, A&A, 458, 441
- Ruzmaikin A., Sokoloff D., Shukurov A., Beck R., 1990, A&A, 230, 284
- Ruzmaikin A. A., Sokoloff D. D., 1979, A&A, 78, 1
- Sokoloff D., Shukurov A., Krause M., 1992, A&A, 264, 396
- Sokoloff D. D., Bykov A. A., Shukurov A., Berkuijsen E. M., Beck R., Poezd A. D., 1998, MNRAS, 299, 189
- Stepanov R., Arshakian T. G., Beck R., Frick P., Krause M., 2008, A&A, 480, 45
- Wolleben M., Landecker T. L., Hovey G. J., Messing R., Davison O. S., House N. L., Somaratne K. H. M. S., Tashev I., 2010, AJ, 139, 1681